

1
2 **Magnetic storm-time red aurora as seen from Hokkaido, Japan on December 1,**
3 **2023 associated with high-density solar wind**

4
5 **Ryuhō Kataoka^{1,2,3}, Yoshizumi Miyoshi⁴, Kazuo Shiokawa⁴, Nozomu Nishitani⁴, Kunihiro**
6 **Keika³, Takanobu Amano³, and Kanako Seki³**

7 ¹National Institute of Polar Research, 10-3 Midori-cho, Tachikawa, Tokyo 190-8518, Japan

8 ²SOKENDAI, Hayama, Kanagawa 240-0193, Japan

9 ³Graduate School of Science, University of Tokyo, 7-3-1 Hongo, Tokyo 113-0033, Japan

10 ⁴ISEE, Nagoya University, Chikusa-ku, Nagoya, Aichi 464-8601, Japan

11
12 Corresponding author: Ryuhō Kataoka (kataoka.ryuho@nipr.ac.jp)

13 **Key Points:**

- 14 • Unusually bright red aurora was witnessed by citizen scientists from Hokkaido, Japan on
15 December 1, 2023.
- 16 • The magnetic storm amplitude was not unusually large, but the solar wind density was
17 extremely high as large as >50 /cc.
- 18 • Asymmetric evolution of the ring current is important to understand the cause of red-
19 aurora magnetic storm events.
20

21 **Abstract**

22 We report a citizen science-motivated study on the cause of an unusually bright red aurora as
23 witnessed from Hokkaido, Japan during a magnetic storm on December 1, 2023. Such an intense
24 red aurora event has occurred in the Halloween 2003 super storm, but the Dst index peak of this
25 December 2023 storm was only -107 nT. In spite of the moderate storm amplitude, the extremely
26 high solar wind density of >50 /cc caused the aurora oval extension to 53 MLAT ($L=2.8$). We
27 discuss that the drift loss of the ring current particles across the small-size magnetopause is
28 important, and Hokkaido was at the right position to see the direct effect of the large particle
29 injection of the storm-time substorm.

30 **Plain Language Summary**

31 Citizen scientists identified an unusually bright red aurora from Hokkaido, Japan during a not-so-
32 unusual magnetic storm on December 1, 2023. This is weird because such an intense red aurora
33 event only occurred in the Halloween 2003 super magnetic storm. The extremely high solar wind
34 density of >50 /cc must be the key to solve this problem. The hypothesis of this study is that the
35 loss of ring current particles across the small-size magnetopause played an important role. Also,
36 we discuss that Hokkaido was at the right position to see the direct effect of storm-time
37 substorm.

38 **1 Introduction**

39 During intense magnetic storms, red auroras can be seen and recorded from middle
40 latitudes like Japan, as the auroral oval expands to lower latitude than usual (Yokoyama et al.,
41 2018; Kataoka and Nakano, 2021). In the historically extreme case, an outstanding red aurora
42 was witnessed and painted from Kyoto, Japan (Kataoka and Iwahashi, 2017). Better
43 understanding of the red aurora appearance, auroral oval extension toward low latitude, and the
44 possible origins and causes are important for improving the space weather forecast of magnetic
45 storm-related hazards such as geomagnetically induced currents in middle latitudes (e.g. Kataoka
46 and Ngwira, 2006).

47 There are at least two different mechanisms to cause the so-called low-latitude auroras.
48 One is called stable red aurora (SAR) arcs, which is related to the heat conduction from the hot
49 ring current ions (Kozyra et al., 1997, Inaba et al., 2021) to cause a pure red line emission at
50 630.0 nm. Another type is called broadband electrons (BBE), which is related to low-to-high
51 energy electrons (tens of eV to several keV) to cause tall curtain-shaped auroras extending up to
52 600 km altitude in the sub-auroral latitude (Shiokawa et al., 1996; 1997). The BBE auroras are
53 extended to so high altitude that the top red part of the aurora can be seen near the north horizon
54 even from the middle latitudes.

55 The origins of such an intense magnetic storm are coronal mass ejections (CMEs)-related
56 solar wind structures. Following the arrival of an interplanetary shock, there is so-called sheath
57 region where the interplanetary magnetic field (IMF) strength and the density was strongly
58 compressed in the shock downstream (Kataoka et al., 2005). Then after the sheath structure, so-
59 called magnetic cloud is occasionally observed, where a smooth rotation of the strong IMF is the
60 marker, although the whole CME-related structure can be complex in some cases.

61 This paper shows the recent example that an bright red aurora was witnessed by naked
62 eyes and also photographed by more than dozen of citizen scientists from Hokkaido, Japan (the
63 northern most region of Japan, and the magnetic latitude of 36~38 deg) on December 1, 2023.

64 Such a naked-eye witness of red aurora is rare in Hokkaido. The last time was 2003 Halloween
65 storm when the Dst index peaked at -383 nT (Kataoka et al., 2017). Therefore, what is truly
66 unusual for this red-aurora event in December 2023 is that the storm amplitude was not so strong
67 and the real-time Dst index peaked at only -107 nT.

68 In this *Letter*, we first show the contribution of the citizen science. We then consult the
69 ground-based and space-born monitoring observation data to discuss the possible mechanisms to
70 cause the unusually bright red-aurora event on December 1, 2023.

71 **2 Red aurora event details**

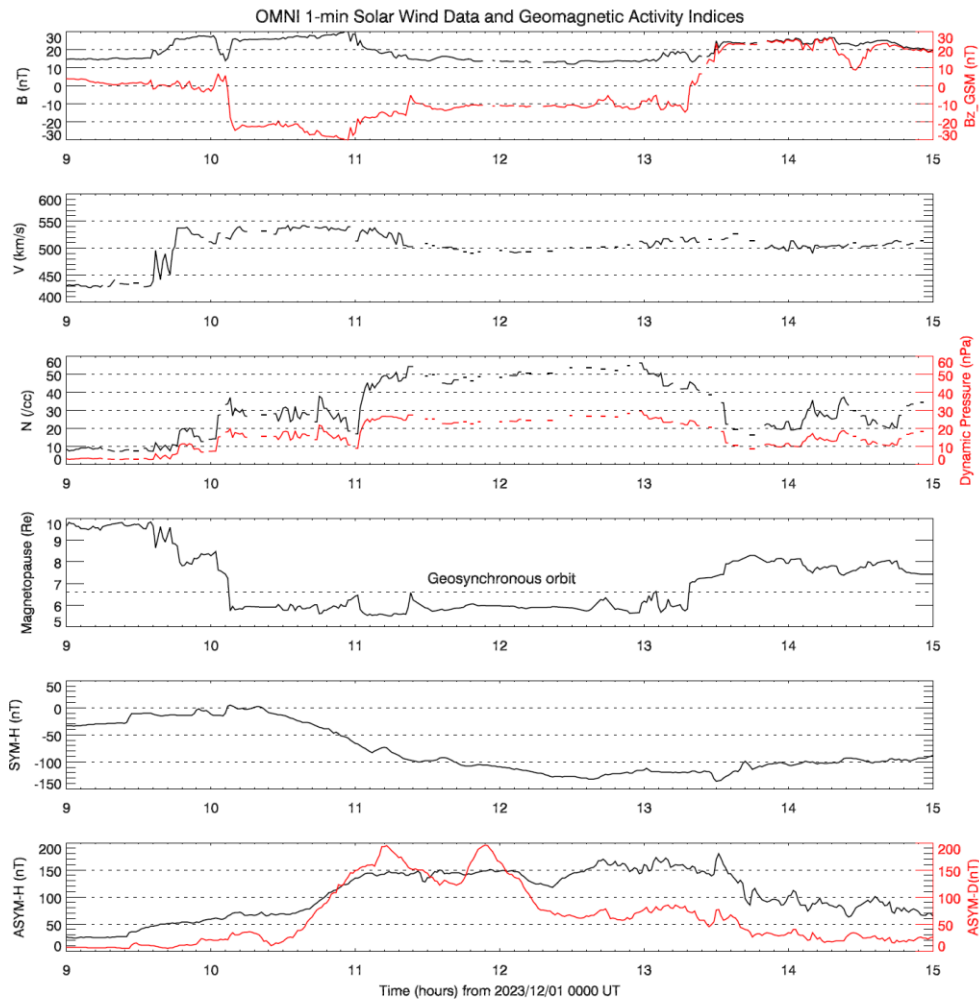
72 The first contribution of the citizen science is that the ray structure was clearly identified
73 in the red aurora. **Figure 1** shows the initial appearance of the red aurora at 1130 UT on
74 December 1, 2023, as taken by the professional photographer KAGAYA. The ray structure
75 indicates the BBE rather than SAR arc.



76
77 **Figure 1.** Red aurora as seen from Bihoro (43.63N, 144.23E, 37.2 MLAT), Hokkaido, Japan at
78 1130 UT on December 1, 2023. (Courtesy of KAGAYA)

79 The solar origin of this magnetic storm was the full-halo CME associated with the M9.8 solar
80 flare occurred around the central meridian position of the Sun at 1930 UT on Nov 28, 2023.
81 More specifically, the magnetic storm on December 1, 2023 was caused by the Earth's arrival of
82 the CME-related interplanetary shock at ~0930 UT, and the strongly compressed solar wind in
83 the shock downstream played the essential role to enhance the geomagnetic activities.

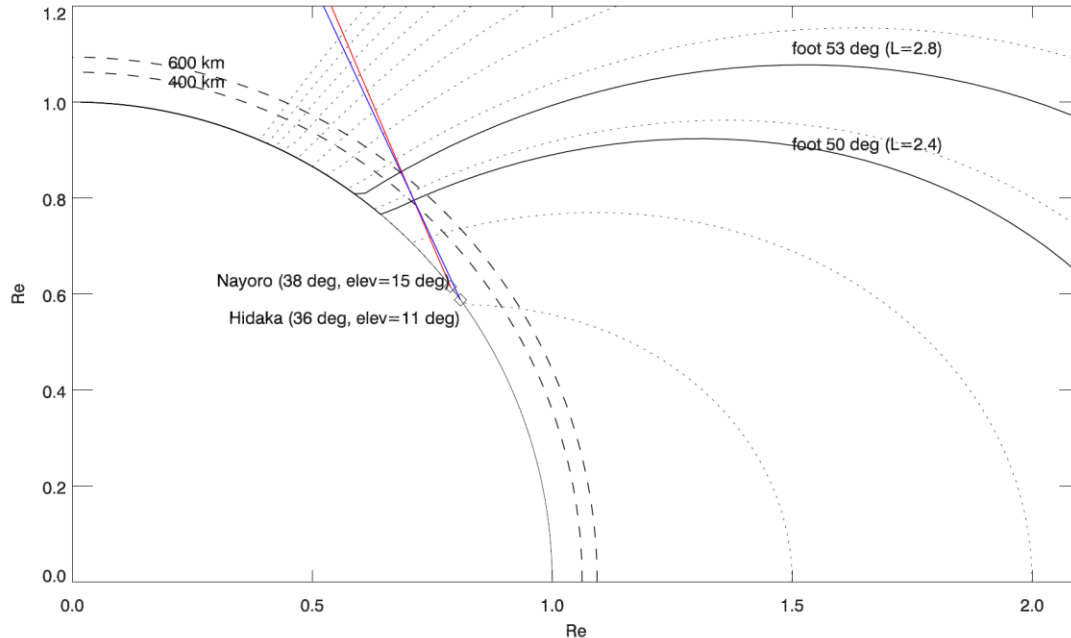
84 **Figure 2** shows the OMNI-2 1-min solar wind data and the SYM-H index. The shock arrival
85 at the magnetopause was at ~0930 UT. In the first stage of the magnetic storm after 1000 UT, the
86 ring current was rapidly developed (the SYM-H index decreased) in an hour due to the strongly
87 southward directing IMF (strong SBZ) of -20 ~ -30 nT. In the second stage after 1100 UT until
88 1330 UT, the SBZ was weakened to -10 nT while the solar wind density was unusually enhanced
89 to >50 /cc. The red aurora was witnessed from Hokkaido for the time interval of 1130-1330 UT.



90

91 **Figure 2.** OMNI-2 solar wind data and geomagnetic activity indices. Top three panels show the
 92 magnetic field (southward component in red), solar wind speed, and density (dynamic pressure in red).
 93 The model magnetopause distance at the subsolar point is also shown. Bottom two panels show the
 94 SYM-H index and ASYM-H index (ASYM-D in red). The time axes of the solar wind parameters were
 95 already shifted as to the magnetopause arrival time to compare with the geomagnetic activity indices.

96 As the second contribution of the citizen science, the photo shootings of the red aurora
 97 obtained at different timing and locations (**Supplemental Information S1**) enable us to estimate
 98 the equatorward edge of the auroral oval as well as the emission height. We identified that the
 99 photos were taken by different persons at close timing at different latitude positions, i.e. from
 100 Nayoro, Hokkaido (1320 UT, 44.34E, 142.38E, 38 MLAT) and from Hidaka (1314 UT, 42.45N,
 101 142.29E, 36 MLAT). Using the stars around the Edasich (Iota Draconis) which appeared to the
 102 north at that time, the elevation angles of the top part of aurora where the color changes from red
 103 to blue were determined to be ~ 15 deg and ~ 11 deg at Nayoro and Hidaka, respectively
 104 (**Supplemental Information S2 and S3**).

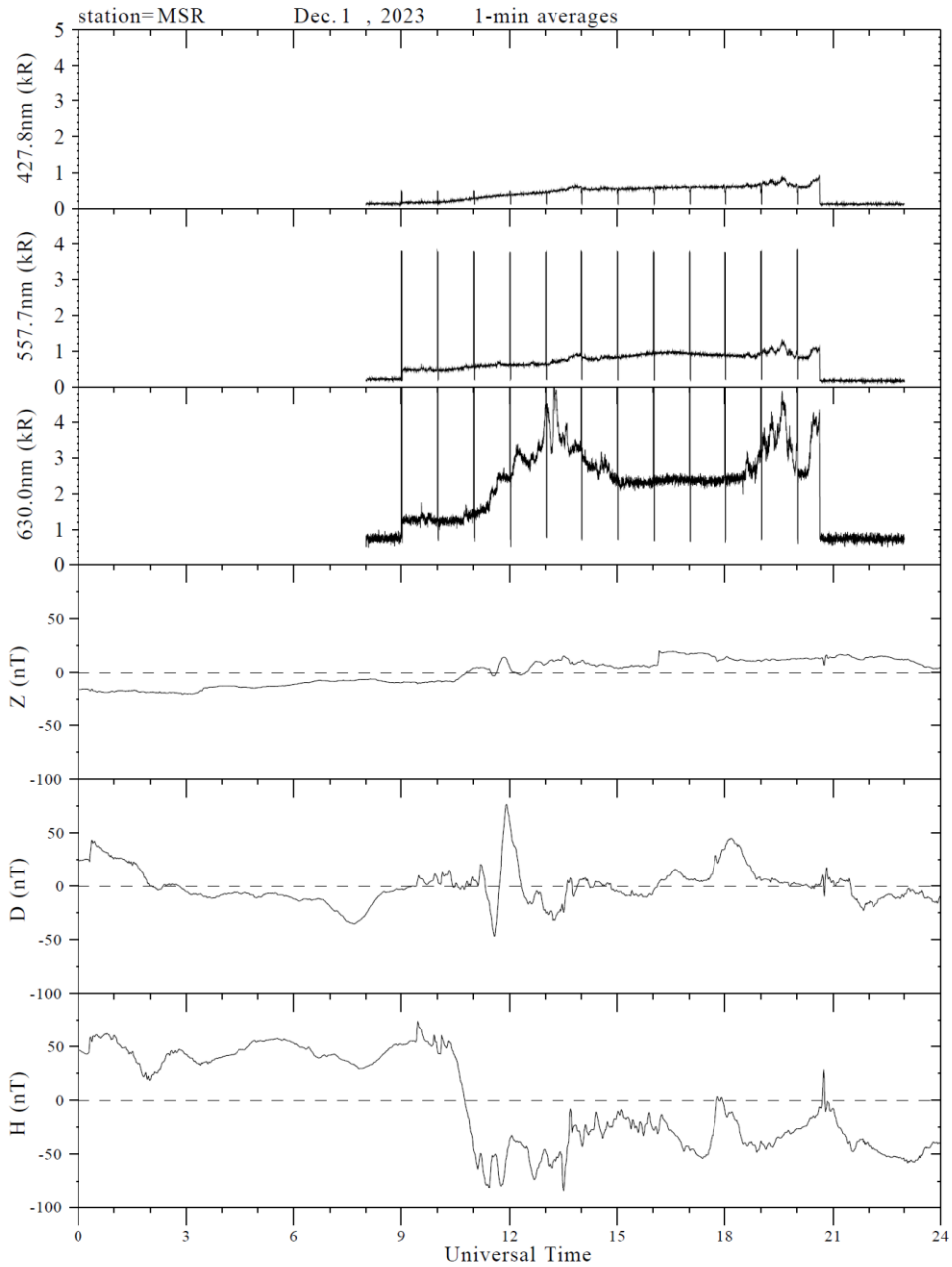


105

106 **Figure 3.** The relationship among the emission altitudes, magnetic field lines of the equatorward edge
 107 of the auroral oval, and observers at ground. The lines-of-sight from Nayoro and Hidaka are denoted
 108 by red and blue lines.

109 Here we draw the dipole magnetic field lines in **Figure 3** to calculate the possible ranges of
 110 auroral oval positions based on these two photographs. As a result, although the ambiguity is
 111 large in this simplest analysis, it is estimated that the top emission altitudes were 400 km to 600
 112 km at the equatorward edge of the auroral oval at 50 deg to 53 deg magnetic latitudes (MLAT),
 113 respectively.

114 Monitoring observations of Nagoya University were also available in Hokkaido area to see
 115 the whole event sequence. **Figure 4** shows the photometer and magnetometer observations at
 116 Moshiri Station, Hokkaido (44.37E, 142.27E, 38 MLAT). Red aurora intensity at 630.0 nm
 117 wavelength was enhanced from 1130 UT to 1330 UT with the peak intensity as large as ~5 kR.
 118 The two-hour time interval (1130-1330 UT) corresponds to the peak time of the magnetic storm
 119 as seen by the H-component depression. Also, there were outstanding large-amplitude negative
 120 and positive peaks in the D-component around 1200 UT. We will come back to this bipolar D-
 121 component variation later again. Similar observation data was also obtained from Rikubetsu
 122 station (**Supplemental Information S4**). Note also that the SuperDARN Hokkaido radar
 123 detected the flow enhancement in the 50~55 MLT range, associated with the red aurora
 124 enhancement ([https://cicr.isee.nagoya-u.ac.jp/cgi-
 125 bin/superdarn/hokkaidowest.cgi?year=2023&month=12&day=01&beam=12&jump=Plot](https://cicr.isee.nagoya-u.ac.jp/cgi-bin/superdarn/hokkaidowest.cgi?year=2023&month=12&day=01&beam=12&jump=Plot)). The
 126 details of the SuperDARN data analysis will be reported elsewhere.



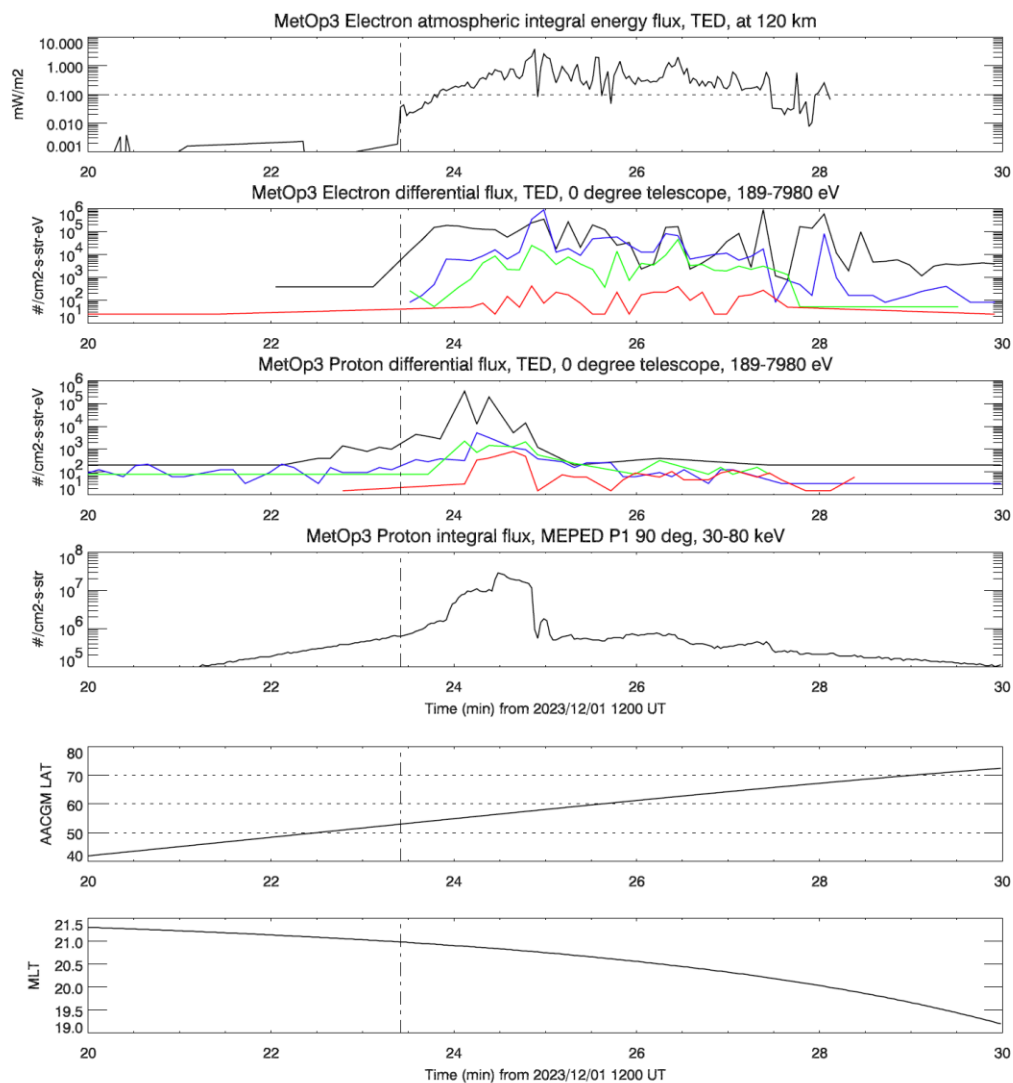
127

128 **Figure 4.** Ground-based monitoring observation at Moshiri Station, Hokkaido. Rapid evolution
 129 of the ring current occurred at 1030-1100 UT (bottom panel, magnetometer H-component). After
 130 the ring current evolution peak, the red auroral intensity was gradually enhanced from 1130 UT
 131 and peaked at 5 kR at 1300-1330 UT (third panel, to geographic north and 15 deg. elevation
 132 angle) when the solar wind density was unusually high. The artificial pulse every hour is for the
 133 brightness calibration. After the pre-heating of the photometer from 0800 UT, the photometer
 134 observation actually started at 0900 UT by opening the shutter.

135

136 **3 Satellite observation across the auroral oval**

137 Fortunately, the MetOp3 satellite orbiting at ~ 830 km altitude passed across the auroral oval
 138 from 40 to 70 MLAT (from 21 to 19 magnetic local time (MLT), the pre-midnight sector
 139 including the Japan's local time and the MLT) at from 1220 to 1230 UT, respectively. The
 140 enhancement of low-energy electrons from 0.2 keV to 8 keV was identified over the auroral
 141 oval. Note that the deeper intrusion of the protons compared to the electrons are not surprising at
 142 this pre-midnight MLT sector. Although the total integral energy flux (**Figure 5**, top panel) was
 143 not beyond the so-called "visible level" of 1 mW/m^2 at the low-latitude boundary, the red aurora
 144 can be visible from ground-based observer via the line-of-sight integration in the current case of
 145 looking toward near the horizon. As shown in the forth panel of **Figure 5**, it is also found that the
 146 ring current particles deeply intruded at around 53~54 MLAT, close to the auroral oval
 147 equatorward boundary.



148

149 **Figure 5.** MetOp3 satellite's data across the auroral oval at the pre-midnight MLT sector. The top
 150 four panels show the total electron energy flux, electron precipitation differential flux, proton
 151 precipitation differential flux, and the trapped proton integral flux at 30-80 keV. The energies of

152 differential fluxes are 189, 844, 2595, and 7980 eV as colored by black, blue, green, and red,
153 respectively. Bottom two panels show the footprint MLAT of the satellite orbit and the MLT.

154 As indicated by the vertical dash-dotted lines at 1223:25 UT, the low-latitude boundary of the
155 auroral oval can be identified at ~ 53 MLAT, and the lowest energy electrons at 189 eV are
156 dominated at the lowest latitude. The low energy electrons are consistent with the red ray-
157 structured aurora as identified from the ground-based photos (**Figure 1**). Yodav et al. (2021)
158 reported the similar characteristic that low energy electrons precipitate at the lowest edge of the
159 auroral oval, which has been considered as one of the important origins of the low-latitude red
160 auroras.

161 **4 Summary and discussions**

162 From the dataset shown above, it is found that the auroral oval actually extended to ~ 53
163 MLAT (**Figure 5**), and the top red part of the auroral oval was witnessed and photographed by
164 citizen scientists in Hokkaido (**Figure 3**). We first discuss that both the equatorward extension of
165 the auroral oval to the 53 MLAT and the brightness of the red aurora were unusual for the
166 relatively small amplitude of this magnetic storm with the Dst index peak at -107 nT.

167 Using the 22-year satellite dataset, Kataoka and Nakano (2021) estimated that possible range
168 of the low-latitude boundary of the auroral oval is 53~57 MLAT for -100 nT Dst levels. The
169 latitude range is along the theoretical curves that the ring current energy corresponds to 10~20 %
170 of the ambient magnetic energy. Therefore, the oval extension of the December 2023 storm
171 locates at the lowest edge of the 22-year statistics.

172 Note also that, even though they were not seen by naked eyes, red auroras have recently been
173 photographed from Hokkaido during the St. Patrik storm on March 17, 2015 (Dst peak -234 nT,
174 630.0 nm brightness ~ 0.5 kR, solar wind density ~ 30 /cc; see Kataoka et al., 2015) and
175 November 5, 2023 storm (Dst peak -172 nT, 630.0 nm brightness ~ 1 kR, solar wind density
176 ~ 30 /cc, see Kataoka and Bamba, 2023). The brightness of the red aurora is therefore 5~10 times
177 larger for the December 2023 event, even though the storm amplitude is much smaller than those
178 of St. Patrik storm and November 2023 storm.

179 The common points of these three storm events are the high solar wind densities and the
180 resultant geosynchronous magnetopause crossing (GMC), i.e. magnetopause size becomes
181 smaller than $6.6 R_E$, occurring at the same time of the red aurora appearance. Although the
182 locations of GOES satellites were not at the right positions to observe the GMC event in the
183 December 2023 storm (GOES spacecraft were in the dawn side), the model calculation (Shue et
184 al., 1998) shows that the December 2023 event could also be under the GMC condition (**Figure**
185 **2**).

186 If we seek the differences, the solar wind density of ~ 50 /cc in the December 2023 event is the
187 largest among these three red aurora events. Further, as shown in **Figure 2**, the ASYM-H index
188 was as large as 150~180 nT, which was 30~50 nT larger than the $|\text{SYM-H}|$ of ~ 130 nT when the
189 red aurora appeared. The large difference between ASYM-H and $|\text{SYM-H}|$ means that the partial
190 ring current was highly evolved. Note here that for both the St. Patrik storm and November 2023
191 storm, $|\text{SYM-H}|$ was larger than ASYM-H during the red aurora timings.

192 In fact, the local storm amplitude ΔH for the December 2023 storm was 141 nT at Japan's
193 Kakioka station, which is significantly larger amplitude than the Dst storm level. Considering the

194 large dynamic pressure of 25 nPa (**Figure 1**), the pressure-corrected ΔH can be 166 nT.
195 Therefore, the storm amplitude was not so small as it looked like from the real-time Dst index.

196 Another unique point of this December 2023 event is the large-amplitude bipolar D-
197 component variation during the red aurora appearance (**Figure 4**), which is related to the
198 unusually large ASYM-D index in **Figure 1**. The bipolar variation can be explained by the
199 expansion and the westward motion of the so-called substorm “current wedge” current system,
200 i.e. the positive and negative D-component peaks at middle latitude correspond to the upward
201 and downward field-aligned currents, respectively. It is common that the red aurora appearance
202 as seen from Japan was associated with storm-time substorms (Shiokawa et al., 1994; 2005), but
203 the unusually large amplitude of the D-component variation for this event indicates that the
204 substorm's current system was located so close to the Earth.

205 In summary, it was found that the unusually bright red aurora in the December 2023 storm
206 was the product of the combinations of 1) extremely high solar wind density (strongly
207 compressed magnetosphere), 2) unusually low-latitude extension of the auroral oval (deep
208 intrusion of ring current particles), 3) large ASYM-H index (asymmetric ring current), and 4) the
209 large-amplitude bipolar D-component variation and unusually large ASYM-D index (near-Earth
210 substorm current system evolution).

211 As the physical mechanism, the drift loss of ring current particles across the magnetopause
212 (e.g., Keika et al., 2005) can naturally connect these four characteristics as follows. Given a
213 strong plasma injection occurred associated with the storm-time substorm (#4), the auroral oval
214 accordingly extended to low latitude associated with the deep intrusion of the ring current
215 particles (#2). The contribution of the injected particles to the magnetic storm amplitude was,
216 however, limited because of the large amount of the drift loss of the ring current particles across
217 the unusually small magnetopause (#1), which also caused the evolution of the largely
218 asymmetric ring current (#3).

219 In additional to the basic hypothesis described above, other different density effects on the
220 auroral oval intensity might also boost the brightness of the December 2023 event. For example,
221 Shue et al. (2002) showed that the density effect of the nightside auroral intensity is strong in the
222 winter season during the SBZ conditions. Therefore, the ionosphere may play some roles,
223 although the exact mechanism has not yet been elucidated. The density effects have also been
224 known as non-linear in the high-latitude auroral current system (Nakano and Kataoka, 2022;
225 Kataoka and Nakano, 2023). In future works, it would therefore be important to investigate the
226 nonlinear density effects on the auroral current system and on the ring current particles in much
227 more details.

228 Lessons learned from this December 2023 red-aurora storm event would be the importance of
229 citizen science not to miss the rare interesting auroral phenomenon, and the importance of
230 consulting the ASYM-H index or local storm amplitude ΔH in addition to the SYM-H or the Dst
231 index to understand the possibly large space weather impacts associated with the GMC events, as
232 well as to fairly evaluate the actual magnitudes of the super magnetic storms causing the red
233 aurora witnesses events such as preserved in the historical records.

234 **Acknowledgments**

235 This work was done by the cooperation of many citizen scientists via X (Twitter), including
236 KAGAYA, Kazuma Saito, Akihiro Takimoto, Kohei Nagira, Yasuo Sano, and Satoru
237 Fukushima. We thank the use of OMNI-2 1 min data via OMNIWeb and the MetOp3 data via
238 NOAA/NCEI. We thank the use of geomagnetic activity indices published from the WDC Kyoto
239 University. This work was supported by the Project of Build an International Collaborative
240 Research for Pre-modern Japanese Texts.

241

242 **Open Research**

243 The OMNI-2 1 min data is available from the OMNIWeb
244 (https://omniweb.gsfc.nasa.gov/ow_min.html). SYM-H, ASYM-H, and ASYM-D indices were
245 obtained from WDC Kyoto University (<https://wdc.kugi.kyoto-u.ac.jp/aeasy/index.html>). The
246 MetOp3 TED and MEPED data were obtained from ([https://www.ncei.noaa.gov/data/poes-
247 metop-space-environment-monitor/access/11b/v01r00/2023/metop03/](https://www.ncei.noaa.gov/data/poes-metop-space-environment-monitor/access/11b/v01r00/2023/metop03/)).

248

249 **References**

250 Inaba, Y., Shiokawa, K., Oyama, S., Otsuka, Y., Connors, M., Schofield, I., et al. (2021). Multi-
251 event analysis of plasma and field variations in source of stable auroral red (SAR) arcs in inner
252 magnetosphere during non-storm-time substorms. *Journal of Geophysical Research: Space
253 Physics*, 126, e2020JA029081. <https://doi.org/10.1029/2020JA029081>

254

255 Kataoka, R., S. Watari, N. Shimada, H. Shimazu, and K. Marubashi (2005), Downstream
256 structures of interplanetary fast shocks associated with coronal mass ejections, *Geophys. Res.
257 Lett.*, 32, L12103, doi:10.1029/2005GL022777.

258

259 Kataoka, R., et al. (2017), Historical space weather monitoring of prolonged aurora activities in
260 Japan and in China, *Space Weather*, 15, 392-402, doi:10.1002/2016SW001493.

261

262 Kataoka, R., & Iwahashi, K. (2017). Inclined zenith aurora over Kyoto on 17 September 1770:
263 Graphical evidence of extreme magnetic storm. *Space Weather*, 15, 1314-1320.
264 <https://doi.org/10.1002/2017SW001690>

265
266 Kataoka, R., and S. Nakano (2021), Auroral zone over the last 3000 years, *J. Space Weather*
267 *Space Clim.*, 11, 46, <https://doi.org/10.1051/swsc/2021030>.

268
269 Kataoka, R., S. Nakano, and S. Fujita (2023), Machine learning emulator for physics-based
270 prediction of ionospheric potential response to solar wind variations, *Earth, Planets and Space*
271 2023 75:139, <https://doi.org/10.1186/s40623-023-01896-3>.

272
273 Kataoka, R., and Y. Bamba (2023), Pileup shocks to cause the red-aurora magnetic storm on
274 November 4-6, 2023. ESS Open Archive, DOI: 10.22541/essoar.170224566.62154907/v1

275
276 Keika, K., M. Nose, S.-I. Ohtani, K. Takahashi, S. P. Christon, and R. W. McEntire (2005),
277 Outflow of energetic ions from the magnetosphere and its contribution to the decay of the storm
278 time ring current, *J. Geophys. Res.*, 110, A09210, doi:10.1029/2004JA010970.

279
280 Kozyra, J. U., A. F. Nagy, and D. W. Slater (1997), High-altitude energy source(s) for stable
281 auroral red arcs, *Rev. Geophys.*, 35(2), 155-190, doi:10.1029/96RG03194.

282
283 Nakano, S. and R. Kataoka (2022), Echo state network model for analyzing solar-wind effects on
284 the AU and AL indices, *Ann. Geophys.*, 40, 11-22, <https://doi.org/10.5194/angeo-40-11-2022>.

285

286 Shue, J.-H., et al. (1998), Magnetopause location under extreme solar wind conditions, *J.*

287 *Geophys. Res.*, 103(A8), 17691-17700, doi:10.1029/98JA01103.

288

289 Shue, J.-H., P. T. Newell, K. Liou, and C.-I. Meng (2002), Solar wind density and velocity

290 control of auroral brightness under normal interplanetary magnetic field conditions, *J. Geophys.*

291 *Res.*, 107(A12), 1428, doi:10.1029/2001JA009138.

292

293 Shiokawa, K., K. Yumoto, Y. Tanaka, T. Oguti, and Y. Kiyama (1994), Low-latitude auroras

294 observed at Moshiri and Rikubetsu ($L = 1.6$) during magnetic storms on February 26, 27, 29, and

295 May 10, 1992, *J. Geomagn. Geoelectr.*, 46, 231-252.

296

297 Shiokawa, K., T. Ogawa, and Y. Kamide (2005), Low-latitude auroras observed in Japan: 1999-

298 2004, *J. Geophys. Res.*, 110, A05202, doi:10.1029/2004JA010706.

299

300 Shiokawa, K., K. Yumoto, C.-I. Meng, G. Reeves, Broadband electrons observed by the DMSP

301 satellites during storm-time substorms, *Geophys. Res. Lett.*, 23, 2529-2532, 1996.

302

303 Shiokawa, K., C.-I. Meng, G. D. Reeves, F. J. Rich, and K. Yumoto (1997), A multievent study

304 of broadband electrons observed by the DMSP satellites and their relation to red aurora observed

305 at midlatitude stations, *J. Geophys. Res.*, 102(A7), 14237-14253, doi:10.1029/97JA00741.

306

307 Yadav, S., Shiokawa, K., Oyama, S., Inaba, Y., Takahashi, N., Seki, K., et al. (2021). Study of
308 an equatorward detachment of auroral arc from the oval using ground-space observations and the
309 BATS-R-US-CIMI model. *Journal of Geophysical Research: Space Physics*, 126,
310 e2020JA029080. <https://doi.org/10.1029/2020JA029080>

311

312 Yokoyama, N., Kamide, Y., and Miyaoka, H. (1998) The size of the auroral belt during magnetic
313 storms, *Ann. Geophys.*, 16, 566-573, <https://doi.org/10.1007/s00585-998-0566-z>.

314